Satellite passive microwaves reveal recent climate-induced carbon losses in African drylands

Brandt, Martin; Wigneron, Jean Pierre; Chave, Jerome; Tagesson, Torbern; Penuelas, Josep; Ciais, Philippe; Rasmussen, Kjeld; Tian, Feng; Mbow, Cheikh; Al-Yaari, Amen; Rodriguez-Fernandez, Nemesio; Schurgers, Guy; Zhang, Wenmin; Chang, Jinfeng; Kerr, Yann; Verger, Aleixandre; Tucker, Compton; Mialon, Arnaud; Rasmussen, Laura Vang; Fan, Lei; Fensholt, Rasmus

Published in:
Nature Ecology and Evolution

DOI:
10.1038/s41559-018-0530-6

2018

Document Version:
Publisher's PDF, also known as Version of record

nature ecology & evolution

ARTICLES

https://doi.org/10.1038/s41559-018-0530-6

Satellite passive microwaves reveal recent climate-induced carbon losses in African drylands

Martin Brandt[1*], Jean-Pierre Wigneron[2*], Jerome Chave[3], Torbern Tagesson[1], Josep Penuelas[4,5], Philippe Ciais[6], Kjeld Rasmussen[1], Feng Tian[1], Cheikh Mbow[7], Amen Al-Yaari[2], Nemesio Rodriguez-Fernandez[8], Guy Schurgers[1], Wenmin Zhang[1,9], Jinfeng Chang[6], Yann Kerr[8], Aleixandre Verger[4,5], Compton Tucker[10], Arnaud Mialon[8], Laura Vang Rasmussen[1], Lei Fan[2] and Rasmus Fensholt[1]

The African continent is facing one of the driest periods in the past three decades as well as continued deforestation. These disturbances threaten vegetation carbon (C) stocks and highlight the need for improved capabilities of monitoring large-scale aboveground carbon stock dynamics. Here we use a satellite dataset based on vegetation optical depth derived from low-frequency passive microwaves (L-VOD) to quantify annual aboveground biomass-carbon changes in sub-Saharan Africa between 2010 and 2016. L-VOD is shown not to saturate over densely vegetated areas. The overall net change in drylands (53% of the land area) was −0.05 petagrams of C per year (Pg C yr^{-1}) associated with drying trends, and a net change of −0.02 Pg C yr^{-1} was observed in humid areas. These trends reflect a high inter-annual variability with a very dry year in 2015 (net change, −0.69 Pg C) with about half of the gross losses occurring in drylands. This study demonstrates, first, the applicability of L-VOD to monitor the dynamics of carbon loss and gain due to weather variations, and second, the importance of the highly dynamic and vulnerable carbon pool of dryland savannahs for the global carbon balance, despite the relatively low carbon stock per unit area.

The forests and savannahs of Africa have attracted particular attention, because both climate change and land-use pressure have large impacts on the carbon stocks of woody vegetation, with immediate consequences for the global carbon balance[1–4]. Deforestation is a well-known threat not only to rainforests[2,5–8], but also to savannah vegetation, which is also threatened by climatic extremes such as dry years[9]. However, the net balance of carbon stocks in the savannah vegetation, changes in plant growth rates (negatively impacted by humans and dry periods but positively affected by elevated CO_2 levels[1]) and altered mortality of the woody vegetation are currently unknown[10,11]. We also do not know whether semi-arid regions in Africa, which were identified as an important carbon sink[12] with a peak in the extremely wet year of 2011[13], have become a carbon source following the recent extreme El Niño in 2015–2016[14]. Knowledge of the amount, distribution and turnover of carbon in African vegetation is crucial for understanding the effects of human pressure and climate change[15], but the shortcomings of optical and radar satellite products and the lack of systematic field inventories have led to considerable uncertainty in documenting patterns of carbon stocks, and their long-term change over the African continent[3,4]. Static carbon maps have been developed based on field plots and satellite data using light detection and ranging (LIDAR), visible/infrared reflectivities and radar backscattering. These maps constitute the best benchmarks to date for carbon stored in living woody vegetation[16–20]. The application of different techniques, however, complicates the direct comparison of these maps, and results differ in magnitude and spatial patterns[19,20]. Importantly, the temporal dynamics of carbon stocks cannot be derived from the above benchmark maps, impeding timely, repeated and reliable carbon assessments[21].

By contrast, the vegetation optical depth (VOD) derived from high frequency (>5 GHz) passive microwave-based satellite systems has been used to monitor changes in vegetation carbon[22,23]. Although the coarse spatial resolution of passive microwaves (43 km gridded at 25 km) has limited their application in the detection of the spatial extent of deforestation, this technology is an attractive alternative to other remote sensing systems, because microwaves at frequencies lower than 15 GHz are almost insensitive to atmospheric and cloud effects. However, high-frequency VOD saturates over forested areas and is generally not considered to be an accurate tool for carbon monitoring[5,7]. The Soil Moisture and Ocean Salinity (SMOS) mission launched in 2009 was the first passive microwave-based satellite system operating at L-band (1.4 GHz) frequency[24]. These low frequencies allow the satellite to sense deeper within the canopy layer with less influence of green non-woody plant components. The VOD derived from SMOS, hereafter L-VOD, is thus less sensitive to saturation effects[25], marking an important step forward in the monitoring of carbon as a natural resource. In this study, we use L-VOD to quantify the inter-annual dynamics of aboveground carbon stocks for the period 2010–2016. This study does not attempt at improving current aboveground carbon stock maps nor at a comparison with state-of-the-art data and maps on carbon stocks[18–20,23].

[1]Department of Geosciences and Natural Resource Management, University of Copenhagen, Copenhagen, Denmark. [2]ISPA, UMR 1391, INRA Nouvelle-Aquitaine, Bordeaux Villenave d'Ornon, France. [3]Laboratoire Evolution and Diversité Biologique, Bâtiment 4R3 Université Paul Sabatier, Toulouse, France. [4]CSIC, Global Ecology Unit CREAF-CSIC-UAB, Bellaterra, Spain. [5]CREAF, Cerdanyola del Vallès, Spain. [6]Laboratoire des Sciences du Climat et de l'Environnement, CEA-CNRS-UVSQ, CE Orme des Merisiers, Gif sur Yvette, France. [7]START International Inc, Washington DC, USA. [8]CESBIO, Université de Toulouse, CNES/CNRS/IRD/UPS, Toulouse, France. [9]International Institute for Earth System Sciences, Nanjing University, Nanjing, China. [10]NASA Goddard Space Flight Center, Greenbelt, MD, USA. *e-mail: mabr@ign.ku.dk; jean-pierre.wigneron@inra.fr

On the basis of calibrated relationships between L-VOD and an existing benchmark map, we present and analyse temporal patterns of gains and losses in different humidity zones of sub-Saharan Africa in response to recent dry years.

Results

Estimating Africa's carbon stocks with passive microwaves. The L-VOD map averaged for 2010–2016 was linearly correlated with a benchmark map of aboveground living biomass carbon (hereafter the term carbon stocks is used) across Africa[19] (Fig. 1a). Although the benchmark map contains bias and uncertainties (Supplementary Fig. 1, Supplementary Table 1), the comparison clearly demonstrates the strong relationship between L-VOD and carbon stocks. The reference map[19] was therefore used as a training set to convert L-VOD to carbon per unit area (Mg C ha^{-1}; $r=0.94$; root mean square error (RMSE) = 11 Mg C ha^{-1}, $P<0.01$, $n=26{,}199$) (Supplementary Figs. 1 and 2). It was previously reported[19] that the total carbon stocks of Africa are 64.50 Pg C (±13 at the 95% confidence level), which was reproduced (Fig. 1b) using L-VOD data, which predicted a carbon stock of 66.95 Pg C (±10 at the 95% confidence level, estimated by 10-fold cross-validated RMSE) for the same spatial extent. In contrast to L-VOD, high-frequency X-band VOD[23] (X-VOD) from Advanced Microwave Scanning Radiometer 2 (AMSR-2) saturated for values that were greater than 100 Mg C ha^{-1} (Fig. 1b) and optical satellite data for values that were greater than 50 Mg C ha^{-1} (Supplementary Fig. 2). Moreover, X-VOD data had a much higher inter-annual variability (0.2 ± 0.16 (mean ± s.d.)) than we observed in the L-VOD data (0.04 ± 0.02 (mean ± s.d.)).

We stratified the L-VOD time series analysis of African vegetation into (1) drylands versus humid areas (as defined by the ratio between annual precipitation and potential evapotranspiration[12]) and (2) four merged land cover classes[26] (Supplementary Figs. 3 and 4, Supplementary Table 1). The ability of L-VOD to predict carbon stocks was of similarly strength for drylands (14.28 ± 3.7 Pg C ($r=0.73$, $P<0.01$, RMSE = 3.4 Mg C ha^{-1}, $n=13{,}418$)) and for humid areas (56.47 ± 8.2 Pg C ($r=0.93$, $P<0.01$, RMSE = 7.9 Mg C ha^{-1}, $n=12{,}781$)). The spatial distribution of carbon stocks at continental scales was relatively even among the land cover classes, with open trees/shrubs (including agricultural lands) comprising almost half of the carbon stocks of rainforests (Supplementary Table 1). The mean carbon density was correlated with mean soil moisture and the mean annual rainfall was correlated with changing classes of land cover along the rainfall gradients (Fig. 1c,d). The correlation between carbon density and rainfall disappears at around 1,600 mm rainfall, and carbon density was markedly higher for rainforests than for the remaining classes (Fig. 1d).

Africa's carbon stocks are highly dynamic. To compute annual changes in carbon stocks, the coefficients derived from the relationship between the aboveground biomass carbon map[19] and mean L-VOD (Fig. 1a) were applied for each yearly median L-VOD map separately. The general relationship between the reference map and annual L-VOD was stable between individual years (Supplementary Fig. 5). The space-for-time substitution was applied, because no inventory data at such a fine temporal resolution were available. Significant trends in carbon were found using per-pixel linear trends in annual carbon density for 2010–2016 ($P<0.05$, 7 years) (Fig. 2a). Carbon net changes (increases and decreases) were computed by comparing the difference in carbon stocks between the years 2010 and 2016 (Supplementary Table 1). Gross losses and gains were calculated by cumulating positive and negative changes between all the consecutive years from 2010 to 2016 (Fig. 2b–f). Gross changes are larger than net changes as losses and recovery occur in the same pixel/region over the study period. The balance between gross gain and gross loss equals the net changes and is shown in Fig. 2b.

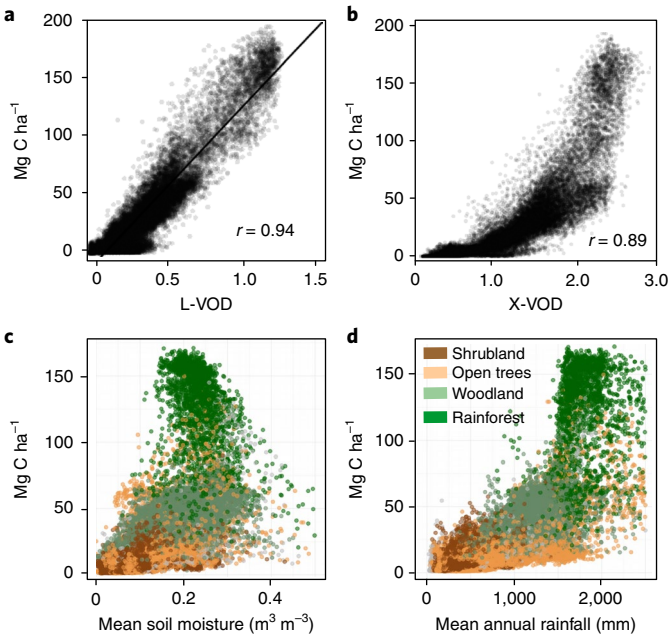

Fig. 1 | Relationships between carbon density in biomass and VOD in sub-Saharan Africa. a, Regression between biomass carbon density from previously published data[19] (obtained from GLAS space-borne data and forest inventories 2007/2008) and average low-frequency L-VOD (2010–2016) from this study, showing no saturation in the relationship. **b**, Same regression with high frequency X-VOD from AMSR-2 (average 2012–2015); this relationship saturates at biomass values that were greater than 100 Mg C ha^{-1}. **c**, Relationship between L-VOD estimated carbon density (mean 2010–2016) and SMOS-IC surface soil moisture (mean 2010–2016). **d**, Relationship between L-VOD estimated carbon density (mean 2010–2016) and mean annual rainfall (CHIRPS) for 2010–2016 (colours attribute a land-cover class to each pixel of 25 × 25 km). Number of pixels for all plots = 26,711.

Over the study period, net changes in carbon were relatively balanced in most latitudinal bands (Fig. 2c). Across sub-Saharan Africa, gross gains (1.57 Pg C yr^{-1}) were offset by gross losses (−1.65 Pg C yr^{-1}) with an overall negative net carbon budget for Africa (−0.10 Pg C yr^{-1}). The majority of the net losses occurred in drylands (−0.05 Pg C yr^{-1}), whereas humid areas experienced a smaller carbon loss (−0.02 Pg C yr^{-1}). Notably, a gross carbon loss of −0.67 Pg C yr^{-1} occurred in drylands and is partly compensated for by a gross gain of 0.62 Pg C yr^{-1}. This gross loss per year represents approximately 5% of the dryland total carbon stocks in Africa (14.28 ± 3.7 Pg C in 2010) (Fig. 2f). By contrast, yearly gross losses from humid areas represent approximately 2% (−0.95 Pg C yr^{-1}) of the total stock (56.47 ± 8.2 Pg C in 2010), with noticable areas in the Democratic Republic of the Congo, Ethiopia, Uganda, Ivory Coast, Ghana and Nigeria (Fig. 2b,d). Gross gains in humid areas were 0.93 Pg C yr^{-1} and were mainly located around the central African forest of the Congo basin (Fig. 2b,c,e,f). The fact that the magnitude of gross fluxes were much larger than that of net fluxes illustrates the highly dynamic variations in carbon stocks during the study period.

Areal and net changes in carbon stocks were close to zero when averaged per land cover class at a continental scale (Fig. 2g). The open trees/shrubs class had gross gains that were below gross losses (net change −0.06 Pg C yr^{-1}; Supplementary Fig. 6, Supplementary Table 1). Using Senegal as a case study site, the observed L-VOD decrease was related to a mass dying of shrubs (2013–2015) caused by a prolonged dry period that was documented by very high spatial-resolution satellite and field data from 2015, see ref. [27] for

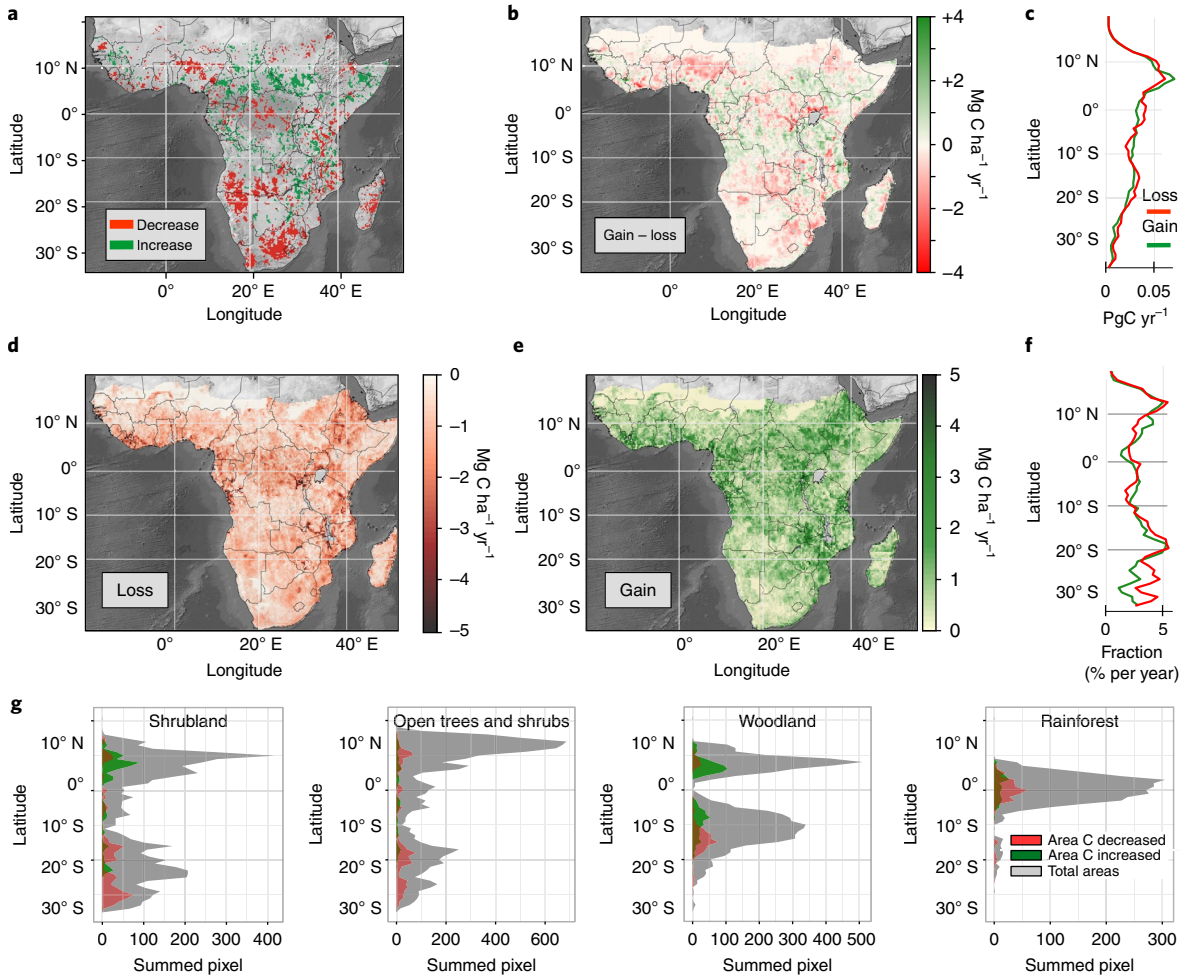

Fig. 2 | Changes in carbon stocks for 2010–2016. a, Pixels with significant ($P<0.05$) positive (green) and negative (red) changes (linear trend; $P<0.05$) in L-VOD as a proxy for aboveground carbon density for the 2010–2016 period. **b**, Net changes in carbon density ($n=26{,}711$) between 2010 and 2016. **c**, latitudinal sums of gross losses and gains. **d**, Cumulative gross losses (time integral of losses) in carbon density. **e**, Cumulative gross gains in carbon density (time interval of gains). **f**, Fractional gross losses and gains per year in the L-VOD data averaged per latitude. **g**, Areas affected by significant ($P<0.05$) positive (green) and negative (red) changes in L-VOD carbon density 2010–2016 summed per latitude band.

further documentation of this event (Fig. 3, Supplementary Fig. 7). Stocks of woodlands considerably increased north approximately 10° S but decreased further south (Fig. 2g), with a continental scale increase of 0.04 Pg C yr^{-1}. Gross losses in rainforests were −0.27 Pg C yr^{-1}, presumably caused by deforestation (Fig. 2b–d). Gross gains (0.24 Pg C yr^{-1}) almost compensated carbon losses in rainforests, but losses occurred on larger areas than gains (Fig. 2g). Using a simple bookkeeping model, an annual carbon loss from deforestation of −0.40 Pg C yr^{-1} in Africa has been reported previously[28], which is comparable to our observed values for rainforests (−0.27 Pg C yr^{-1}), although belowground biomass carbon changes and delayed soil carbon emissions after deforestation, which were part of the bookkeeping model, were not included in the L-VOD-based carbon estimates.

For individual years, the largest net losses (−0.69 Pg C for all Africa, −0.25 for drylands and −0.44 Pg C for humid areas) were found in 2015 (Fig. 4a), which is comparable to the net carbon fluxes that were measured by the Orbiting Carbon Observatory-2 for tropical Africa (−0.80 Pg C) during the severe El Niño[29]. Although the losses in drylands were considerable, the losses observed in humid areas in 2015 were approximately twice as high, as this was the driest year of the study period. Overall positive net changes were observed between 2011 (0.15 Pg C) and 2013 (0.17 Pg C). Net changes in 2011 were negative in drylands (−0.18 Pg C) but positive in humid areas (0.34 Pg C).

We applied two ecosystem models to test the performance of state-of-the-art methods that are commonly used to assess large-scale temporal carbon dynamics. The spatial patterns of carbon stored in aboveground woody vegetation simulated by the Lund–Potsdam–Jena General Ecosystem Simulator (LPJ-GUESS; $r=0.85$, $P<0.01$) and the Organizing Carbon and Hydrology in Dynamic Ecosystems–Ameliorated Interactions between Carbon and Temperature (ORCHIDEE-MICT; $r=0.87$, $P<0.01$) agreed reasonably well with L-VOD carbon estimations (Fig. 4b, Supplementary Fig. 2). Drylands, however, showed a share of the total pool of African carbon stocks of 20% in L-VOD but only 6% in LPJ-GUESS and 8% in ORCHIDEE-MICT, possibly because these models describe vegetation as either grass or tree plant functional types, but do not incorporate the mixed types that occur in savannahs. Inter-annual variations in LPJ-GUESS-simulated carbon stocks were comparable with L-VOD estimates for the years 2011–2013, but carbon losses in 2015 were strongly underestimated by the model (Fig. 4a). Net changes in 2014 were positive in the ecosystem model, but negative in L-VOD. Average annual variations in C density (Mg C ha^{-1}) were 1.5 ± 1.1 (mean ± s.d.) when calculated using L-VOD and 1.1 ± 1.5 (mean ± s.d.) using LPJ-GUESS.

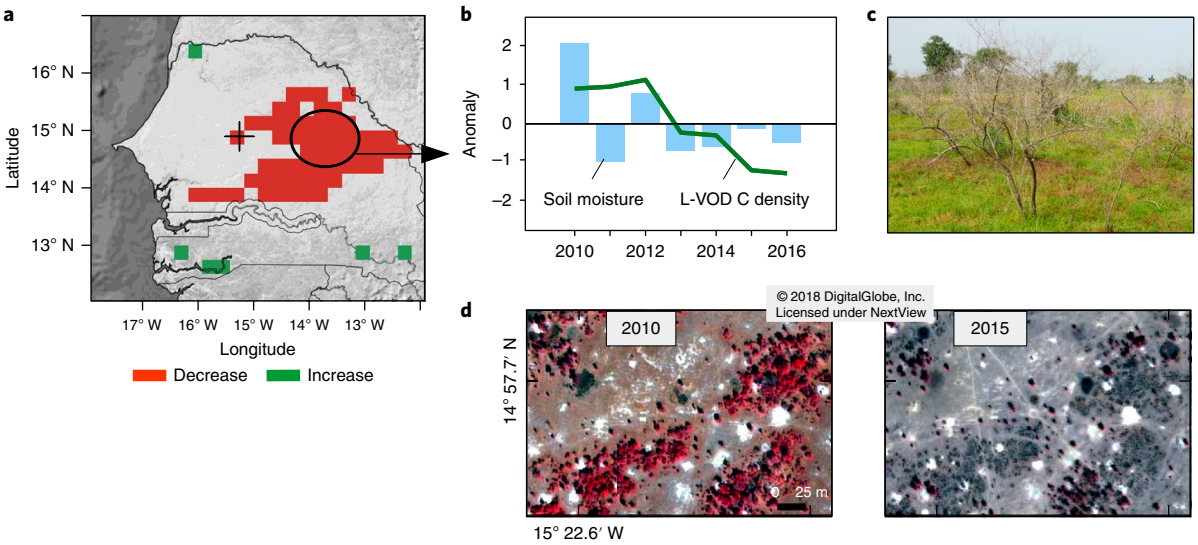

Fig. 3 | Shrub die-off in Senegal. a, Pixels with significant changes (linear trend; $P < 0.05$) in L-VOD carbon density (2010–2016). **b**, L-VOD carbon density (average of pixels in the circle) decreased rapidly after 2013, reflecting widespread mortality of *Guiera senegalensis* shrubs between 2013 and 2015 due to a prolonged dry period. **c**,**d**, This event was documented by field photos (**c**, 2015) and very high spatial resolution satellite imagery (**d**, from the WorldView-2 and QuickBird-2 satellites; Supplementary Fig. 7). The cross in **a** marks the location of the very high spatial resolution images.

Recent dry periods have reduced carbon stocks in dryland areas. The soil moisture data[30] showed latitudinal patterns that were similar to L-VOD carbon density data and explained a large fraction of the observed dynamics in carbon stocks between 2010 and 2016 (Fig. 5a,b). Although the fire frequency increased in 2016, fewer fires occurred in areas of major L-VOD decreases (Fig. 5c). These recent decreases in L-VOD-estimated carbon stocks were most pronounced in southern Africa, which was approximately reproduced by the ecosystem models (Fig. 5d,e). Moreover, rainfall data[31] and vegetation greenness indicated abnormally dry conditions in most parts of Africa in recent years, particularly during the severe El Niño episode of 2015–2016 (Fig. 5f,g), indicating that dry years have caused the changes in L-VOD, rather than impacts from human disturbance and fires. Prior to 2010, conditions were stable and extraordinarily positive anomalies in carbon density and soil moisture were recorded for 2011 (Fig. 5a,b), confirming previous studies based on ecosystem models and greenness satellite data[13]. In the later years, carbon stocks estimated by L-VOD and simulated by ecosystem models decreased considerably (Fig. 5b,d,e) and southern Africa turned from being a carbon sink into a source, with considerable carbon losses between 2014 and 2016. Simulations by ecosystem models suggested that the negative trend in dryland carbon stocks persisted over the 1982–2015 period, beyond the SMOS observation era (Fig. 5h–j). Simulated increases in humid areas around 5° N–10° S were less strong in L-VOD (Fig. 5e), but observed decreases around 0° were not shown in the climate-driven ecosystem models, suggesting that deforestation was the cause.

Overall, most of the detected decreases in carbon stocks were related to the abnormally low soil moisture (Fig. 6a) and rainfall

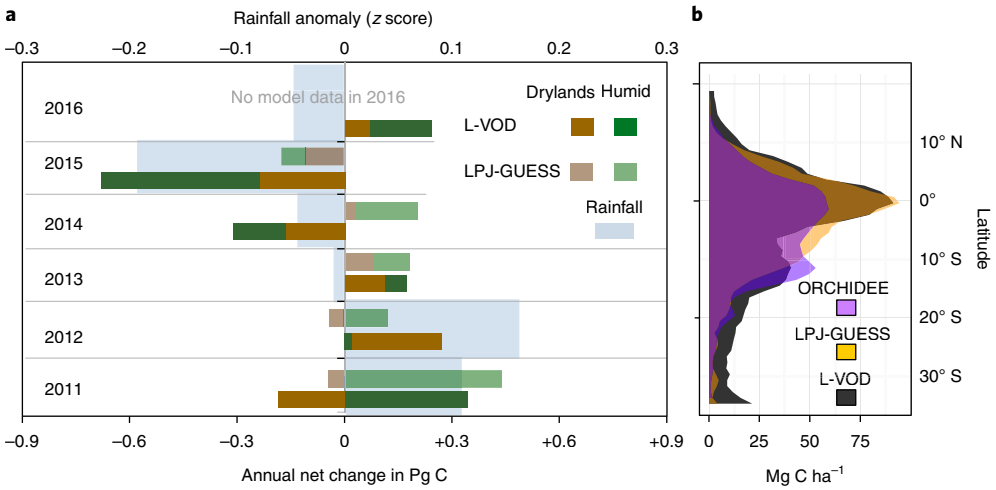

Fig. 4 | Observed and simulated carbon dynamics. a, Net carbon changes for individual years (compared to the previous year) observed by L-VOD and simulated by LPJ-GUESS. Model results for the year 2016 could not be displayed because harmonized gridded climate forcing data were not available at the time of this analysis. CHIRPS annual rainfall anomalies (*z* score calculated over the period 1981–2016) are shown in light blue. **b**, Latitudinal averages of L-VOD carbon density (dark grey) compared to LPJ-GUESS-simulated (orange) and ORCHIDEE-MICT-simulated (purple) values of aboveground biomass carbon.

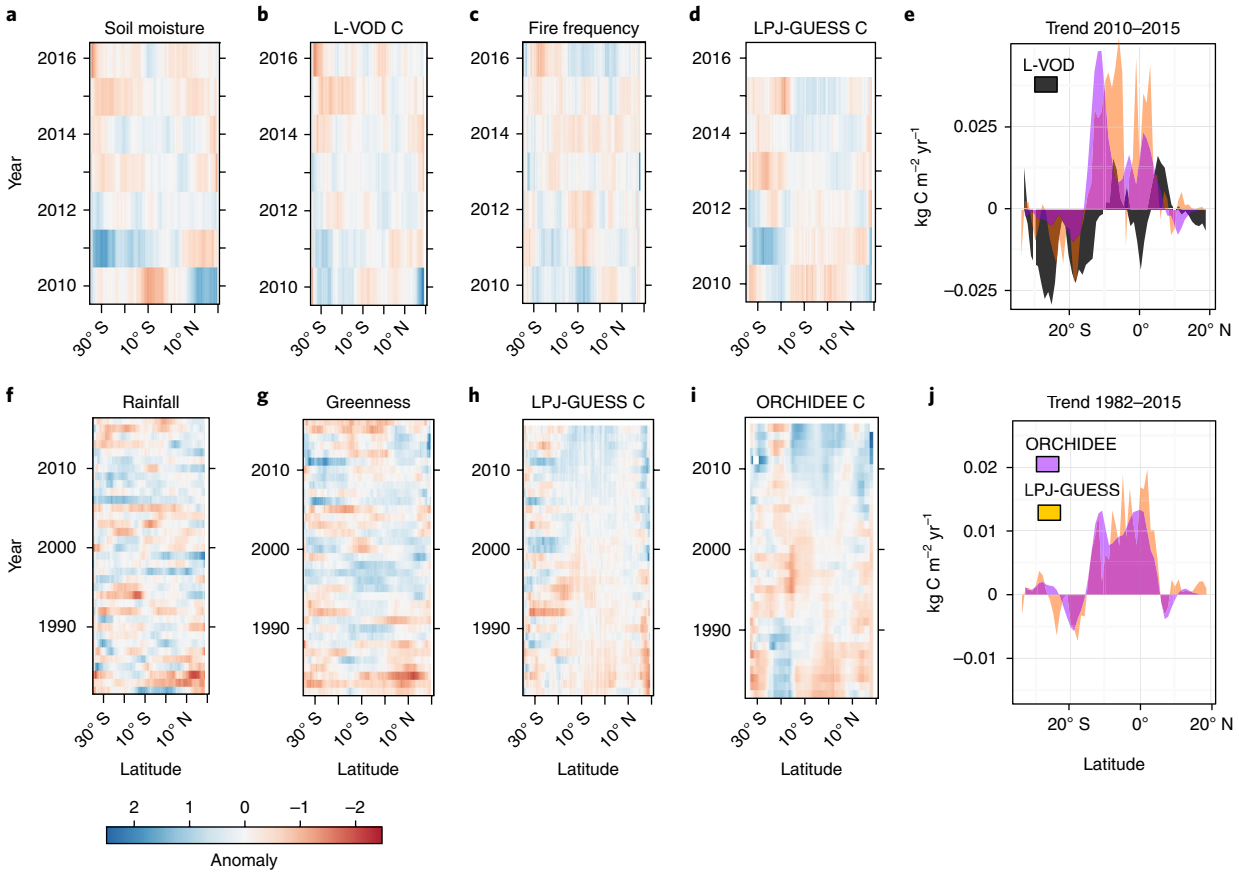

Fig. 5 | Hovmöller diagrams showing anomalies (*z* score) for Africa for each year and latitude. a–d, Anomalies for 2010–2016 in SMOS soil moisture (**a**), L-VOD carbon density (**b**), MOD14CMH fire frequency (**c**) and LPJ-GUESS-simulated aboveground woody carbon density (**d**). Model results for the year 2016 could not be displayed because harmonized gridded climate forcing data were not available to drive these models at the time of this analysis. **e**, Trend (linear regression slope) for the aboveground carbon density simulated by the ecosystem models and observed in the L-VOD model (2010–2015). **f–i**, Anomalies for 1982–2016 in the number of rainy days (>1 mm) (**f**), vegetation greenness (annually summed normalized difference vegetation index (NDVI)) (**g**) and carbon density simulated with the ecosystem models LPJ-GUESS (**h**) and ORCHIDEE-MICT (**i**). **j**, Linear trends for the aboveground carbon density in the ecosystem models (1982–2015).

conditions (Fig. 6b). Note, however, that soil moisture cannot explain the large-scale increases in carbon for around 5° N that may either reflect non-symmetrical net primary productivity responses to wet years (positive convexity), improved forest management or a decrease in wood-fuel gathering in regions affected by conflicts and migration to urban areas (such as, South Sudan and the Central African Republic). At the country scale, carbon stocks were found to increase in Sudan, the Central African Republic, Cameroon, Chad and Zimbabwe (Fig. 6b), in spite of mostly dry conditions and marked deforestation reported by the FAO in these countries[32]. Carbon stocks decreased considerably in Ghana, Ivory Coast, Nigeria, Uganda and Kenya, which may have partly been caused by deforestation. Despite their lower woody covers compared to forested areas, large losses of carbon were found in South Africa, and were related to dry years.

The sensitivity of inter-annual variability in carbon density to dry years was assessed by a Spearman rank correlation between carbon density and soil moisture (Fig. 6c, Supplementary Fig. 8). This showed that country level carbon stocks were less sensitive to dry years in countries with humid regions whereas stocks were most sensitive in countries with drylands.

Discussion

Assessing aboveground carbon stocks and their changes using repeated inventories with a gridded sampling scheme is laborious and impossible to implement in all African countries, so assessments with short intervals for understanding changes in stocks from year to year are unrealistic at a continental scale[17]. SMOS-IC L-VOD data provide a valuable alternative and a tool for rapid monitoring of carbon stocks and their changes. Our comparison with an existing benchmark map[19] provided highly satisfactory correlations, supporting the utility of the data. The coarse spatial resolution (25 km) sets clear limits for the operational application of the L-VOD dataset in relation to local scale forest monitoring. In addition, this work is based on early prototype VOD-retrieval algorithms that are not free of uncertainty. However, this study shows that low-frequency VOD is a major leap forward to enable assessments of carbon dynamics at the regional to global scale. Furthermore, the applied benchmark map inevitably includes propagated uncertainty (Supplementary Table 1), and the conversion adds some uncertainty to the final prediction. However, a deviation of L-VOD does not imply that the benchmark map is closer to reality. An independent calibration of L-VOD with field surveys, LIDAR and very high spatial resolution imagery for a stand-alone biomass product is a logical next step. For this study, however, the strong correlation between L-VOD and the benchmark map enabled us to provide an application of low-frequency passive microwaves to estimate temporal changes in carbon units at the sub-continental scale. The method that was used in this study is preferable to optical remote sensing, because

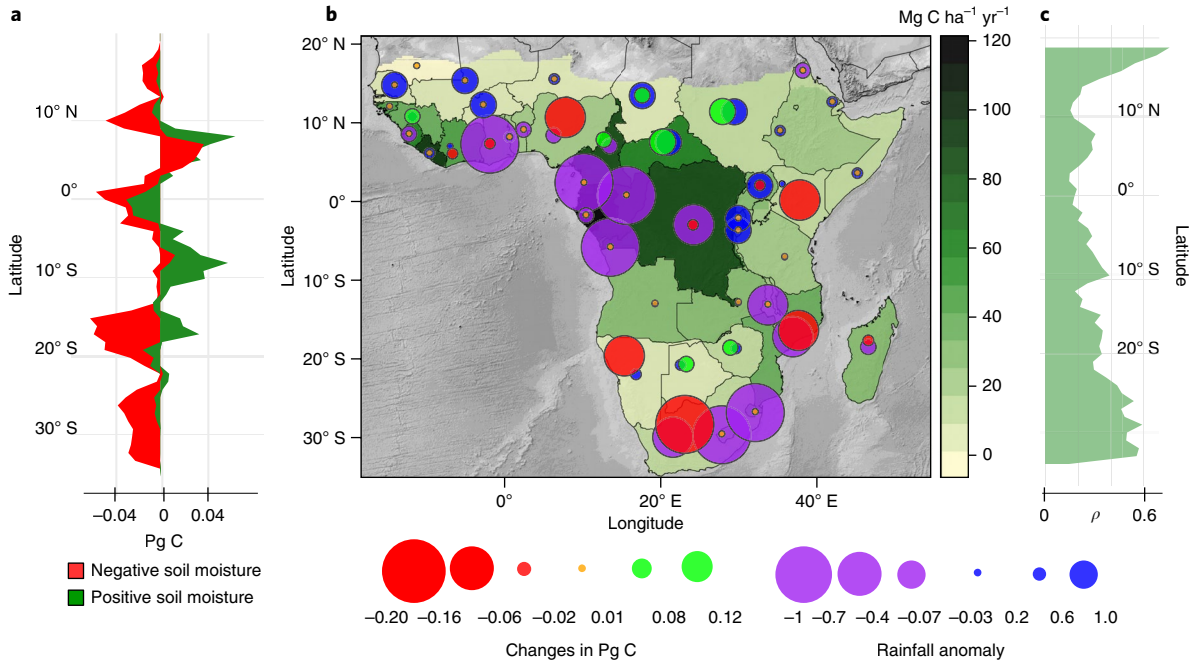

Fig. 6 | Climate as a driver of carbon stock dynamics. a, Direction and magnitude of net carbon change for 2010–2016 (summed per latitude) are shown for areas with positive (green) and negative (red) linear trends in soil moisture (2010–2016). **b**, Average carbon density (in Mg C ha^{-1}) and net carbon change for 2010–2016 summed for each country (in Pg C). Anomalies in annual rainfall (2010–2016 compared to 1981–2016) averaged for each country are shown as purple (negative anomaly) and blue (positive anomaly) circles. **c**, Correlations between annual carbon stocks and annual soil moisture (shown as Spearman's ρ, $n = 26{,}711$) averaged along the latitudes.

the L-VOD data are only controlled by the biomass of the vegetation and do not seem to saturate in forests. Moreover, although high-frequency X-VOD has been successfully used for global biomass mapping[23], the X-VOD sensor is more sensitive to green vegetation and restricted to the upper green canopy layer when the vegetation is dense[22]. This is visible from a much higher inter-annual variability in mean annual values of X-VOD than those that we observed using L-VOD, and the intra-annual variations of monthly L-VOD data are also low (mean (±s.d.) amplitude of 0.01 ± 0.01). Therefore, the advantage of L-VOD over previous methods is that it enables the continuous monitoring of carbon stocks, annually or even more frequently, for both forests and savannahs. Our results demonstrate the potential utility of L-VOD as a complementary data source for the quantification and monitoring of carbon stocks for national reports and large-scale efforts, such as the United Nations Framework Convention on Climate Change (UNFCCC) and the Intergovernmental Panel on Climate Change (IPCC), especially for semi-arid regions with little inventory data.

Continuing deforestation and forest degradation supposedly contributed to the gross carbon losses observed in humid areas, in particular in rainforests and woodlands. Forest degradation does not strongly reduce carbon stocks and is followed by permanent recovery, and future studies therefore need to explore whether this process may be concealed by saturation or whether it can be detected using L-VOD.

In spite of carbon losses that are presumably caused by deforestation, we found that carbon stocks in rainforests remained relatively stable over the period of 2010–2016 and were not evidently correlated with variations in rainfall and soil moisture. On the other hand, carbon stocks outside densely forested areas were much more variable and were highly sensitive to climatic fluctuations, with two extreme events that consisted of a very wet year in 2011 and a very dry one in late 2015 and early 2016. Previous studies[1,13,33] have often reported global increases in dryland carbon stocks, which has led to the general understanding that drylands may serve as carbon sinks. Our study found that dry years have partly reversed this trend for 2010–2016 in areas in which such increases in woody vegetation (and thus carbon stocks) have occurred in the past (for example southern and west Africa[1,33–35]), demonstrating that climate controls short-term variations in carbon stocks at large scales.

Previous studies of carbon dynamics in Africa were based on ecosystem models and optical satellite observations that measure changes in the green fraction rather than in biomass. Our observational data on dryland vegetation carbon stocks and dynamics showed substantially higher values than simulated in the two ecosystem models, suggesting that models may underestimate the crucial role of dryland savannahs as carbon sinks and sources[13,34,36]. The losses of carbon from African drylands during 2010–2016 support the view that the large area of drylands and their highly variable carbon stocks make these ecosystems important to the global accounting of the carbon balance, even though mean carbon stocks are generally quite low per area unit. With such inter-annual variability, it is difficult to conclude from the 7 years of observation presented here whether the observed trends reflect quasi-decadal variations or whether it is a sign of longer-term dynamics. However, considerable losses were observed in 2010–2016, so we need to reassess whether, in the long term, woody vegetation in African savannahs will indeed continue to be a carbon sink[37]. If dry years become more frequent[38], large-scale carbon losses may exacerbate climate change, particularly in dry areas. Our study therefore highlights the importance of timely monitoring of both tropical deforestation and the highly dynamic woody carbon stocks of savannah ecosystems for assessments of global carbon stocks.

Methods

Passive microwaves for soil moisture, VOD and carbon estimation. The estimations of biomass were computed from the SMOS L-VOD ascending product

in the IC version (1.05)[39]. It is a global product gridded at 25-km spatial resolution and one-day temporal frequency. The SMOS products (soil moisture and L-VOD) are computed from a two-parameter inversion of the L-MEB model (L-band microwave emission of the biosphere) from the multi-angular and dual-polarized SMOS observations[25,40]. Soil moisture and L-VOD products are independent and weakly correlated (Fig. 1c). In the newly developed IC version, these products are independent of the use of auxiliary data from other space-borne observations or simulations from atmospheric models (only surface temperature estimates from ECMWF (European centre for medium-range weather forecasts) products are used in the L-MEB inversion). We applied several steps of filtering to retrieve relatively robust and stable annual estimates. First, we excluded daily observations for which the RMSE between measured and L-MEB modelled values was larger 8 K[39] as well as outliers larger than 2 s.d. from the mean. Then, water bodies and pixels with on average less than 20 valid observations per year were masked out from the analysis. The remaining daily L-VOD values were aggregated to yearly (median) values for 2010–2016. If less than 50 observations were valid for a particular year, the pixel values of these years were replaced by the long-term mean. This left 83% (2010), 93% (2011), 93% (2012), 90% (2013), 90% (2014), 93% (2015) and 92% (2016) of pixels with sufficient observations per year that were used for the analysis. SMOS L-VOD was then converted to carbon density using the previously published biomass map[19] (which was obtained with Geoscience Laser Altimeter System (GLAS) space-borne data, forest inventories and Moderate Resolution Imaging Spectroradiometer (MODIS) data from 2007–2008, which was a period of normal rainfall conditions, see Fig. 5) as a reference (aggregated to 25 km by averaging) by a linear regression with mean L-VOD (2010–2016). To avoid negative values, the regression line was forced through zero: annual median L-VOD values were multiplied with the coefficient 124 to retrieve the unit carbon density. Assuming that approximately 50% of the aboveground vegetation biomass consists of carbon, biomass was converted to carbon by using a fixed factor of 0.5[20,41]. The coefficients from the regression were used to convert L-VOD into carbon density (Mg C ha^{-1}), which was then applied separately to each year from 2010 to 2016 to quantify the dynamics in Mg C ha^{-1}. Conversion to carbon stocks was achieved by multiplying carbon density with the amount of hectare covered by a pixel. Carbon stock statistics per land-cover/humidity class were derived by summing the values of the pixels.

Uncertainty. Owing to the coarse spatial resolution of the SMOS data, a pixel may contain a mix of deforestation, regeneration, livestock pressure, conservation, fires, shrub encroachment and other events, resulting in a mix of carbon gains and losses that cannot be singled out. Moreover, different land cover types (for example, forests, cropland and savannahs) are often mixed within a single pixel. The coarse spatial resolution therefore renders the clear attribution of carbon changes to specific events impossible, unless they are large scale events (such as, climate perturbations). Our analysis thus presents the results of large scale averages (for example, latitudinal) and concentrates on temporal rather than spatial variations. Furthermore, although annual median values have been shown to be stable, remaining noise in the data (for example, radio frequency interferences) cannot be excluded, and may locally affect inter-annual variations. It is, however, unlikely that averages per latitude, land cover class or per humidity zone are biased by noise, which is supported by the very low inter- and intra-annual variations of L-VOD (on average 0.04 and 0.2, respectively).

We did not aim to improve existing biomass maps nor did we assume that the values of the benchmark map were free of errors and represent reality. The benchmark map includes propagated uncertainties from allometric equations, the LIDAR model and the random forest extrapolation[19]. These uncertainties are shown in Supplementary Table 1 and the numbers have to be taken into account when interpreting the results; we refer to the original study[19] for further details. Furthermore, the conversion of L-VOD to carbon density propagates uncertainty that was assessed by a 10-fold cross validation. Here the data were randomly split in 10 folds of equal size, which were used to predict the omitted values. The root of the mean squares of all folds gives the cross-validated RMSE. We report the median RMSE at the 95% confidence level for different classes as $\pm xy$; for a full list, see Supplementary Table 1.

Yearly anomalies were calculated by the z score: (value − mean)/standard deviation. Net carbon changes were estimated by the difference between the carbon maps of 2010 and 2016. Gross losses (gains) were calculated by cumulating negative (positive) differences between the consecutive years, enabling the quantification of the effect of deforestation (or dry years) without considering regeneration. That calculation assigns a per-pixel deforestation fraction per pixel and per year, with a corresponding amount of carbon regrowth that is deduced from the deforestation rate during the next year.

As for L-VOD, soil moisture from the SMOS mission[30] was applied in the IC version[40]. A 30-day median was averaged for each year as a robust proxy for available soil moisture in the root zone. Although soil moisture was derived from the same sensor as L-VOD, the variables are independent attributable to the multi-angular capabilities of the SMOS sensor[42] and Fig. 1c shows that the correlation between soil moisture and L-VOD is weak.

Rainfall data. We used Climate Hazards Group Infrared Precipitation with Station (CHIRPS; v.2) daily rainfall data[31], aggregated to SMOS resolution (average). The number of rainy days per year were counted as days with rainfall >1 mm. Yearly anomalies in rainfall and soil moisture were calculated using the z score: (value − mean)/standard deviation.

Land cover and humidity classes. The European Space Agency's (ESA's) Climate Change Initiative (CCI) L4 land cover[26] for 2015 was aggregated from 300 m to 25 km using a stepwise hierarchical majority aggregation (six steps). We reduced the number of classes to four (open trees/shrubs, shrubland, woodland and rainforest), sorted by potentially increasing woody cover and carbon density. We merged all classes that have scattered trees and shrubs in the class open trees/shrubs, which includes croplands along all rainfall zones, open trees, sparse vegetation and grassland. Note that areas converted from forest to cropland (for example, in west Africa and Madagascar) are therefore included in this class, which also includes remnants of forests, that is, cropland/forest mosaics (Supplementary Fig. 3). Moreover, owing to the large pixel size, a pixel free of trees or shrubs does not exist. Shrublands potentially have a dense woody cover, but the general capacity to store C is low because of the small size of the shrubs. Woodlands included open and closed tree cover, mostly located in the sub-humid and humid zones. This includes the Miombo woodlands. Rainforest are closed forest areas around the equator and at the west African coast, located in areas above 1,500 mm rainfall per year.

Additional data. Commercial satellite data were available via the NextView licence from DigitalGlobe Inc. and were used for illustration (Fig. 3 and Supplementary Fig. 7). The images were from the WorldView-2 and QuickBird-2 satellites and included multispectral imagery, which were pansharpened to a spatial resolution of 50 cm[27]. GIMMS-3g NDVI was used as a proxy for vegetation greenness. We summed the bi-monthly NDVIs for each year for 1982–2016. This is a widely used method to estimate the annual activity of green vegetation[43]. Annual fire frequency was derived from MOD14CMH by averaging monthly values.

Ecosystem models. ORCHIDEE (organizing carbon and hydrology in dynamic ecosystems) is a process-based dynamic global vegetation model that was developed for simulating carbon fluxes, and water and energy fluxes in ecosystems, from site level to global scale[44]. In this study, an updated version known as ORCHIDEE-MICT (ameliorated interactions between carbon and temperature) revision 4080 was run on an African grid using the 6-hourly Climate Research Unit (CRU) and National Centers for Environmental Prediction (NCEP) reconstructed climate data at 2°×2° spatial resolution[44,45,J]. The ESA CCI land cover product[26] for the year 2010 was used to produce a plant functional type map used in ORCHIDEE-MICT model, following previously described methodology[46,47]. An updated release of the historical land-use forcing dataset LUHv2h (http://luh.umd.edu/data.shtml; updated from LUHv1[48]) was applied to this reference plant functional type map to constrain the land-cover changes of forest, natural grassland, pasture and cropland during the period 1860–2015 using the backward method (BM3) according to a previously published study[49]. The simulation run for this study used forced vegetation distribution maps and outputs on woody carbon density (sap- and heartwood) were resampled to L-VOD resolution (bilinear).

LPJ-GUESS[50] is a dynamic vegetation model that simulates the global distribution of vegetation as well as the carbon and nitrogen cycling within vegetation and soils. It applies a set of 12 plant functional types with different morphological, phenological and physiological characteristics, of which 10 represent tree types and 2 represent herbaceous vegetation. For the simulation of woody aboveground biomass, LPJ-GUESS was forced with monthly gridded meteorological station data at a spatial resolution of 0.5°×0.5° from the climatic research unit of the University of East Anglia (CRU ts 3.24.01[51]), monthly model-derived estimates of nitrogen deposition[52] and annual atmospheric CO_2 concentration based on ice core data and atmospheric observations[53,54] in a simulation for the period of 1901–2015. The simulation was preceded by a 500-year spinup applying the first 30 years from the climate forcing in a repeated manner. Land use was represented with a simple implementation following a previously published study[34], applying historical reconstructions of land use from previously published data[48]. Annual maps of woody carbon density (sap- and heartwood) were resampled to L-VOD resolution (bilinear).

Reporting Summary. Further information on experimental design is available in the Nature Research Reporting Summary linked to this article.

Data availability. CHIRPS rainfall data are freely available at the climate hazard group (http://chg.geog.ucsb.edu/data/chirps/). SMOS-IC datasets are available via CATDS (Centre Aval de Traitement des Données SMOS) at http://www.catds.fr/Products/Available-products-from-CEC-SM/SMOS-IC. Also available for public use are soil moisture and L-VOD in the versions L3 and L4 at CATDS (https://www.catds.fr/). The previously published biomass map[19], including an uncertainty map, are freely available from Global Forest Watch. Model results and the L-VOD carbon maps are available from the authors upon request.

Received: 19 October 2017; Accepted: 7 March 2018;
Published online: 09 April 2018

References

1. Brandt, M. et al. Human population growth offsets climate-driven increase in woody vegetation in sub-Saharan Africa. *Nat. Ecol. Evol.* **1**, 0081 (2017).
2. Rudel, T. K. The national determinants of deforestation in sub-Saharan Africa. *Phil. Trans. R. Soc. B* **368**, 20120405 (2013).
3. Ciais, P. et al. The carbon balance of Africa: synthesis of recent research studies. *Phil. Trans. R. Soc. A* **369**, 2038–2057 (2011).
4. Williams, C. A. et al. Africa and the global carbon cycle. *Carbon Balance Manag.* **2**, 3 (2007).
5. Rodriguez-Veiga, P., Saatchi, S., Wheeler, J., Tansey, K. & Balzter, H. in *Earth Observation for Land and Emergency Monitoring* (ed. Balzter, H.) Ch. 2, 5–32 (John Wiley & Sons, Chichester, 2017).
6. Réjou-Méchain, M. et al. Local spatial structure of forest biomass and its consequences for remote sensing of carbon stocks. *Biogeosciences* **11**, 6827–6840 (2014).
7. Reiche, J. et al. Combining satellite data for better tropical forest monitoring. *Nat. Clim. Change* **6**, 120–122 (2016).
8. Hansen, M. C. et al. High-resolution global maps of 21st-century forest cover change. *Science* **342**, 850–853 (2013).
9. Hill, M. J. & Hanan, N. P. *Ecosystem Function in Savannas: Measurement and Modeling at Landscape to Global Scales* (CRC Press, Boca Raton, London, New York, 2010).
10. Allen, C. D. et al. A global overview of drought and heat-induced tree mortality reveals emerging climate change risks for forests. *For. Ecol. Manage.* **259**, 660–684 (2010).
11. Niang, I. et al. in *Climate Change 2014: Impacts, Adaptation, and Vulnerability* (eds Field, C. B. et al.) 1199–1265 (IPCC, Cambridge Univ. Press, 2014).
12. Bastin, J.-F. et al. The extent of forest in dryland biomes. *Science* **356**, 635–638 (2017).
13. Poulter, B. et al. Contribution of semi-arid ecosystems to interannual variability of the global carbon cycle. *Nature* **509**, 600–603 (2014).
14. Yue, C. et al. Vegetation greenness and land carbon-flux anomalies associated with climate variations: a focus on the year 2015. *Atmos. Chem. Phys.* **17**, 13903–13919 (2017).
15. Carvalhais, N. et al. Global covariation of carbon turnover times with climate in terrestrial ecosystems. *Nature* **514**, 213–217 (2014).
16. Mermoz, S., Le Toan, T., Villard, L., Réjou-Méchain, M. & Seifert-Granzin, J. Biomass assessment in the Cameroon savanna using ALOS PALSAR data. *Remote Sens. Environ.* **155**, 109–119 (2014).
17. Gibbs, H. K., Brown, S., Niles, J. O. & Foley, J. A. Monitoring and estimating tropical forest carbon stocks: making REDD a reality. *Environ. Res. Lett.* **2**, 045023 (2007).
18. Saatchi, S. S. et al. Benchmark map of forest carbon stocks in tropical regions across three continents. *Proc. Natl Acad. Sci. USA* **108**, 9899–9904 (2011).
19. Baccini, A. et al. Estimated carbon dioxide emissions from tropical deforestation improved by carbon-density maps. *Nat. Clim. Change* **2**, 182–185 (2012).
20. Avitabile, V. et al. An integrated pan-tropical biomass map using multiple reference datasets. *Glob. Change Biol.* **22**, 1406–1420 (2016).
21. *Adoption of the Paris Agreement* (UNFCCC, 2015).
22. Tian, F. et al. Remote sensing of vegetation dynamics in drylands: evaluating vegetation optical depth (VOD) using AVHRR NDVI and in situ green biomass data over West African Sahel. *Remote Sens. Environ.* **177**, 265–276 (2016).
23. Liu, Y. Y. et al. Recent reversal in loss of global terrestrial biomass. *Nat. Clim. Change* **5**, 470–474 (2015).
24. Kerr, Y. H. et al. Overview of SMOS performance in terms of global soil moisture monitoring after six years in operation. *Remote Sens. Environ.* **180**, 40–63 (2016).
25. Wigneron, J.-P. et al. Modelling the passive microwave signature from land surfaces: a review of recent results and application to the L-band SMOS & SMAP soil moisture retrieval algorithms. *Remote Sens. Environ.* **192**, 238–262 (2017).
26. Hollmann, R. et al. The ESA climate change initiative: satellite data records for essential climate variables. *Bull. Am. Meteor. Soc.* **94**, 1541–1552 (2013).
27. Brandt, M. et al. Woody vegetation die off and regeneration in response to rainfall variability in the West African Sahel. *Remote Sens* **9**, 39 (2017).
28. Houghton, R. A. & Nassikas, A. A. Global and regional fluxes of carbon from land use and land cover change 1850–2015. *Glob. Biogeochem. Cycles* **31**, 456–472 (2017).
29. Liu, J. et al. Contrasting carbon cycle responses of the tropical continents to the 2015–2016 El Niño. *Science* **358**, eaam5690 (2017).
30. Kerr, Y. H. et al. Soil moisture retrieval from space: the soil moisture and ocean salinity (SMOS) mission. *IEEE Trans. Geosci. Remote Sens.* **39**, 1729–1735 (2001).
31. Funk, C. et al. The climate hazards infrared precipitation with stations—a new environmental record for monitoring extremes. *Sci. Data* **2**, 150066 (2015).
32. *Global Forest Resource Assessment* (FAO, 2016).
33. Skowno, A. L. et al. Woodland expansion in South African grassy biomes based on satellite observations (1990–2013): general patterns and potential drivers. *Glob. Change Biol.* **23**, 2358–2369 (2017).
34. Ahlström, A. et al. The dominant role of semi-arid ecosystems in the trend and variability of the land CO_2 sink. *Science* **348**, 895–899 (2015).
35. Stevens, N., Erasmus, B. F. N., Archibald, S. & Bond, W. J. Woody encroachment over 70 years in South African savannahs: overgrazing, global change or extinction aftershock? *Phil. Trans. R. Soc. B* **371**, 20150437 (2016).
36. Biederman, J. A. et al. CO_2 exchange and evapotranspiration across dryland ecosystems of southwestern North America. *Glob. Change Biol.* **23**, 4204–4221 (2017).
37. Mbow, C. Biogeoscience: Africa's greenhouse-gas budget is in the red. *Nature* **508**, 192–193 (2014).
38. Ji, F., Wu, Z., Huang, J. & Chassignet, E. P. Evolution of land surface air temperature trend. *Nat. Clim. Change* **4**, 462–466 (2014).
39. Fernandez-Moran, R. et al. SMOS-IC: an alternative SMOS soil moisture and vegetation optical depth product. *Remote Sens.* **9**, 457 (2017).
40. Wigneron, J.-P. et al. L-band microwave emission of the biosphere (L-MEB) model: description and calibration against experimental data sets over crop fields. *Remote Sens. Environ.* **107**, 639–655 (2007).
41. Chave, J. et al. Tree allometry and improved estimation of carbon stocks and balance in tropical forests. *Oecologia* **145**, 87–99 (2005).
42. Kerr, Y. H. et al. The SMOS soil moisture retrieval algorithm. *IEEE Trans. Geosci. Remote Sens.* **50**, 1384–1403 (2012).
43. Fensholt, R. et al. Greenness in semi-arid areas across the globe 1981–2007 — an Earth Observing Satellite based analysis of trends and drivers. *Remote Sens. Environ.* **121**, 144–158 (2012).
44. Krinner, G. et al. A dynamic global vegetation model for studies of the coupled atmosphere-biosphere system. *Glob. Biogeochem. Cycles* **19**, GB1015 (2005).
45. Wei, Y. et al. The North American Carbon Program Multi-scale Synthesis and Terrestrial Model Intercomparison Project - Part 2: Environmental driver data. *Geosci. Model Dev.* **7**, 2875–2893 (2014).
46. Poulter, B. et al. Plant functional type mapping for earth system models. *Geosci. Model Dev.* **4**, 993–1010 (2011).
47. Poulter, B. et al. Plant functional type classification for earth system models: results from the European Space Agency's land cover climate change initiative. *Geosci. Model Dev.* **8**, 2315–2328 (2015).
48. Hurtt, G. C. et al. Harmonization of land-use scenarios for the period 1500–2100: 600 years of global gridded annual land-use transitions, wood harvest, and resulting secondary lands. *Climatic Change* **109**, 117 (2011).
49. Peng, S. et al. Sensitivity of land use change emission estimates to historical land use and land cover mapping. *Glob. Biogeochem. Cycles* **31**, 626–643 (2017).
50. Smith, B. et al. Implications of incorporating N cycling and N limitations on primary production in an individual-based dynamic vegetation model. *Biogeosciences* **11**, 2027–2054 (2014).
51. Harris, I., Jones, P. D., Osborn, T. J. & Lister, D. H. Updated high-resolution grids of monthly climatic observations – the CRU TS3.10 dataset. *Int. J. Climatol.* **34**, 623–642 (2014).
52. Lamarque, J.-F. et al. Multi-model mean nitrogen and sulfur deposition from the atmospheric chemistry and climate model intercomparison project (ACCMIP): evaluation of historical and projected future changes. *Atmos. Chem. Phys.* **13**, 7997–8018 (2013).
53. Etheridge, D. M. et al. Natural and anthropogenic changes in atmospheric CO_2 over the last 1000 years from air in Antarctic ice and firn. *J. Geophys. Res. Atmos.* **101**, 4115–4128 (1996).
54. Keeling, C. D., Whorf, T. P., Wahlen, M. & van der Plichtt, J. Interannual extremes in the rate of rise of atmospheric carbon dioxide since 1980. *Nature* **375**, 666–670 (1995).

Acknowledgements

This research work was funded by CNES (Centre National d'Etudes Spatiales) through the Science TEC (Terre Environment et Climat) program. M.B., F.T. and R.F. acknowledge the funding from the Danish Council for Independent Research (DFF) Grant ID: DFF–6111-00258. M.B. is supported by an AXA post-doctoral fellowship. We thank DigitalGlobe for providing commercial satellite data within the NextView license program. P.C., A.V. and J.P. acknowledge funding from the European Research Council Synergy grant ERC-2013-SyG-610028 IMBALANCE-P. T.T. was funded by the Swedish national space board (Dnr: 95/16). P.C. acknowledges additional support from the ANR ICONV CLAND grant. J.Chav. has benefited from "Investissement d'Avenir" grants managed by the French Agence Nationale de la Recherche (CEBA, ref. ANR-10-LABX-25-01 and TULIP, ref. ANR-10-LABX-0041), and from TOSCA funds from the CNES.

Author contributions

J.-P.W., M.B., J.Chav., F.T. and R.F. designed the study. J.-P.W., A.A.-Y., N.R.-F., Y.K. and A.M. prepared the SMOS-IC data. P.C. and J.Chan. prepared the ORCHIDEE data, G.S.

prepared the LPJ-GUESS data, C.T. prepared the high spatial-resolution satellite data. M.B., F.T. and W.Z. analysed the data. The results were interpreted by J.Chav., J.-P.W., T.T., J.P., P.C., L.V.R., K.R., C.M., L.F., A.V. and R.F. The manuscript was drafted by M.B., K.R., J.Chav., R.F., J.P.W. and P.C. with contributions by all authors.

Competing interests

The authors declare no competing interests.

Additional information

Supplementary information is available for this paper at https://doi.org/10.1038/s41559-018-0530-6.

Correspondence and requests for materials should be addressed to M.B. or J.-P.W.

nature research

Corresponding author(s): Martin Brandt, Jean Pierre Wigneron

Life Sciences Reporting Summary

Nature Research wishes to improve the reproducibility of the work that we publish. This form is intended for publication with all accepted life science papers and provides structure for consistency and transparency in reporting. Every life science submission will use this form; some list items might not apply to an individual manuscript, but all fields must be completed for clarity.

For further information on the points included in this form, see Reporting Life Sciences Research. For further information on Nature Research policies, including our data availability policy, see Authors & Referees and the Editorial Policy Checklist.

Please do not complete any field with "not applicable" or n/a. Refer to the help text for what text to use if an item is not relevant to your study.
For final submission: please carefully check your responses for accuracy; you will not be able to make changes later.

Experimental design

1. Sample size

   Describe how sample size was determined. — As this is a remote sensing study, all available pixels were used for analyses.

2. Data exclusions

   Describe any data exclusions. — No data were excluded.

3. Replication

   Describe the measures taken to verify the reproducibility of the experimental findings. — The analyses can be reproduced.

4. Randomization

   Describe how samples/organisms/participants were allocated into experimental groups. — We applied land cover and humidity classes to group the pixels.

5. Blinding

   Describe whether the investigators were blinded to group allocation during data collection and/or analysis. — NA

Note: all in vivo studies must report how sample size was determined and whether blinding and randomization were used.

6. Statistical parameters

   For all figures and tables that use statistical methods, confirm that the following items are present in relevant figure legends (or in the Methods section if additional space is needed).

n/a	Confirmed	
☐	☒	The exact sample size (*n*) for each experimental group/condition, given as a discrete number and unit of measurement (animals, litters, cultures, etc.)
☐	☒	A description of how samples were collected, noting whether measurements were taken from distinct samples or whether the same sample was measured repeatedly
☐	☒	A statement indicating how many times each experiment was replicated
☐	☒	The statistical test(s) used and whether they are one- or two-sided *Only common tests should be described solely by name; describe more complex techniques in the Methods section.*
☐	☐	A description of any assumptions or corrections, such as an adjustment for multiple comparisons
☐	☒	Test values indicating whether an effect is present *Provide confidence intervals or give results of significance tests (e.g. P values) as exact values whenever appropriate and with effect sizes noted.*
☐	☒	A clear description of statistics including central tendency (e.g. median, mean) and variation (e.g. standard deviation, interquartile range)
☐	☐	Clearly defined error bars in all relevant figure captions (with explicit mention of central tendency and variation)

See the web collection on statistics for biologists for further resources and guidance.

Software

Policy information about availability of computer code

7. Software

Describe the software used to analyze the data in this study.	GRASS GIS, R, GDAL

For manuscripts utilizing custom algorithms or software that are central to the paper but not yet described in the published literature, software must be made available to editors and reviewers upon request. We strongly encourage code deposition in a community repository (e.g. GitHub). *Nature Methods* guidance for providing algorithms and software for publication provides further information on this topic.

Materials and reagents

Policy information about availability of materials

8. Materials availability

Indicate whether there are restrictions on availability of unique materials or if these materials are only available for distribution by a third party.	SMOS IC data will be made available within a few weeks via CATDS (Centre Aval de Traitement des Données SMOS). A similar data set is already available via CATDS (SMOS L3).

9. Antibodies

Describe the antibodies used and how they were validated for use in the system under study (i.e. assay and species).	NA

10. Eukaryotic cell lines

a. State the source of each eukaryotic cell line used.	NA
b. Describe the method of cell line authentication used.	NA
c. Report whether the cell lines were tested for mycoplasma contamination.	NA
d. If any of the cell lines used are listed in the database of commonly misidentified cell lines maintained by ICLAC, provide a scientific rationale for their use.	NA

Animals and human research participants

Policy information about studies involving animals; when reporting animal research, follow the ARRIVE guidelines

11. Description of research animals

Provide all relevant details on animals and/or animal-derived materials used in the study.	NA

Policy information about studies involving human research participants

12. Description of human research participants

Describe the covariate-relevant population characteristics of the human research participants.	NA